High-Q Whispering-Gallery-Mode-Based Plasmonic Fano Resonances in Coupled Metallic Metasurfaces at Near Infrared Frequencies

*Govind Dayal, Xin Yu Chin, Cesare Soci, and Ranjan Singh**

Fano resonances in metallic and dielectric structures have received much attention in recent years due to their promising applications in surface enhanced phenomena, sensing, and nonlinear optics. The lossless high refractive index dielectric structures have been shown to have ultranarrow resonances at near infrared and optical frequencies. However, it is rather challenging to realize such narrow Fano resonances using metallic nanostructures due to large optical losses in metals that cause significant broadening of the plasmonic resonances. Herein, whispering gallery mode based sharp Fano resonances are demonstrated experimentally and numerically in plasmonic nanostructures at near infrared frequencies with highest quality factor. The design here consists of conductively coupled annular and rectangular aperture arrays that support multiple Fano resonances. The sharp Fano resonances are observed for both the orthogonal polarizations of the incident electric field due to the coupling between quadrupolar resonance of the annular aperture with the dipolar and quadrupolar resonance of the rectangular aperture. The response of the plasmonic metasurface can be switched from single to multiple Fano resonances by switching the polarization of the incident radiation which is highly desirable for hyperspectral sensing and imaging. The spectral tuning of Fano resonances are further achieved by tailoring the coupling between the annular and the rectangular apertures.

1. Introduction

It is well known that metallic nanostructures can sustain surface plasmons that are coherent oscillations of surface charge density at the interface between metal and dielectric materials.[1,2] The harmonic oscillation of the surface charge density in metallic nanostructures, commonly known as the localized surface plasmons (LSPRs), is driven by electric field component of light.[3,4] The spectral response of the localized surface plasmon resonance is extremely sensitive to the nanoparticle composition, their size and shape as well as the dielectric properties of the local environment.[5] Confinement of plasmon modes to a surface of metal nanostructures under the constraints imposed by the finite boundaries of the nanostructure alters their dispersion, only allowing for discrete solutions. In the quasi-static limit, where the wavelength of the excitation light is much larger than the size of the nanostructure, the nanostructure experiences a spatially constant field, and the plasmon mode with a dipolar charge distribution couples strongly with the incident light. As the wavelength of the excitation becomes comparable to the size of the nanostructure, the light electric field can no longer be assumed to be spatially constant inside the particle, and higher order (quadrupole, octupole, etc.) plasmon modes can also be excited due to the phase retardation effect.[3] When resonant metallic nanostructure is illuminated at resonance frequency, notably deep subwavelength optical field confinement produces huge enhancement of electric field amplitude. This property forms the basis of generating and manipulating subwavelength enhanced electromagnetic fields that can govern, control, and improve physical processes such as single molecule detection,[6,7] vibrational spectroscopy,[8] photovoltaic energy conversion,[9] energy transfer,[10] molecular sensing,[11] nanoscale optical signal interconnection,[12] photoemission,[13] and nanoscale microscopy.[14]

An important feature of interest is the quality factor of the plasmonic resonances which is defined as the ratio of the resonance frequency f_0 and the full width at half-maximum (FWHM) bandwidth δf of the Fano resonance. The quality factor ($Q = f_0/\delta f$) of the plasmonic resonances is determined by the losses in the system, namely, the radiative and nonradiative losses. The nonradiative (Ohmic) losses are due to the lifetimes of electron scattering processes, which are mainly electron–electron, electron–phonon, and electron–defect scattering in the material. Radiative losses, on the other hand, can be effectively controlled as the radiation efficiency for higher order modes (quadrupole, octupolar, etc.) is usually much weaker than the dipolar mode. Hence, with suppressed radiative loss, the quality factors of the higher order resonances, in principle, can be engineered to have a higher value which significantly increases

Dr. G. Dayal, X. Y. Chin, Prof. C. Soci, Prof. R. Singh
Center for Disruptive Photonic Technologies
Division of Physics and Applied Physics
School of Physical and Mathematical Sciences
Nanyang Technological University
21 Nanyang Link, Singapore 637371
E-mail: ranjans@ntu.edu.sg

DOI: 10.1002/adom.201600356

© 2016 WILEY-VCH Verlag GmbH & Co. KGaA, Weinheim

the life-time of the resonance and thus reduces its line width due to the contribution of intrinsic damping. The fundamental dipolar mode of a nanostructure couples efficiently with the incoming light and is classified as super-radiant (bright mode) in contrast to higher order LSPRs, which are not easily excited by light at normal incidence and are classified as sub-radiant (dark mode). It has been demonstrated that the higher order plasmon resonance of nanostructures can be excited at normal incidence (nonretarded case) through asymmetric coupling by breaking the structural symmetry or at an oblique angle of incidence illumination (retarded case).[15] The asymmetry[16] in the system leads to a complex charge distribution inside the nanostructure which can be understood in terms of the hybridization of dipolar and other higher order modes.[17] Hence, the realization of high-*Q* plasmonic devices strongly depends on our ability to control these radiative and nonradiative losses. Many fundamental studies such as selective thermal emitters, nonlinear studies and applications such as ultrasensitive label-free chemical and bimolecular detection[18,19] are still at early stage of development and would get a strong boost from planar plasmonic resonant devices with a higher quality factor.

Over the past few years, a new approach has been discovered to realize sharp spectral features in plasmonic nanostructures and metamaterials with the characteristics of asymmetric properties in the scattered line shape which occurs due to the spectral overlap of a super-radiant (bright mode) and sub-radiant (dark mode) phenomena in wave scattering. Such asymmetric shape resonances were first observed in a quantum mechanical study of the autoionizing states of atoms by Fano in 1961.[20] Fano predicted the asymmetric shape of such spectral lines based on the superposition between two scattering channels involving a continuum and a discrete state. In case of plasmonic nanostructure and metamaterials,[21,22] a radiative dipolar mode (bright mode) that can be directly excited in the system serves as the continuum and a narrow band (dark mode) resonance acts as the discrete mode. Fano resonance in metamaterials was first observed in artificially structured arrays of asymmetrical split-ring at microwave frequencies.[23] Since then, a number of structural designs such as disk-ring cavities,[24–26] self-assembled metal nanostructure heptamers and quadrumers,[27,28] and dolmen structures[29] have been demonstrated to exhibit Fano resonances across the electromagnetic spectrum ranging from microwave,[23] terahertz,[30–33]infrared,[34] and optical domain.[29] Despite the tremendous progress in the exploration of Fano resonances in plasmonic metal based nanostructures, the achievable *Q*-factors at optical and near infrared (NIR) frequencies have been less than 10.[35] However, recently high-*Q* Fano resonances were observed in dielectric based periodic arrays.[36,37]

2. Discussion

In this paper, we present an approach to excite plasmonic whispering gallery modes in a metallic nanostructure to significantly enhance the *Q*-factor of the Fano resonance at NIR frequencies. Here, we demonstrate a Fano resonant plasmonic nanostructure with the highest simulated and experimental *Q*-factor values of 79 and 38, respectively. The high-*Q* Fano resonances are enabled by the excitation of plasmonic whispering gallery modes. Our proposed plasmonic structure consists of an array of conductively coupled annular and rectangular apertures as shown in **Figure 1**. Both annular and rectangular aperture arrays have been studied in great detail due to their extraordinary transmission properties by exciting surface plasmon polaritons (SPPs).[38] In particular, annular aperture array have been shown to have superior transmission properties as compared to a hole array owing to their ability of supporting both the localized and propagating surface plasmons.[39] Due to the

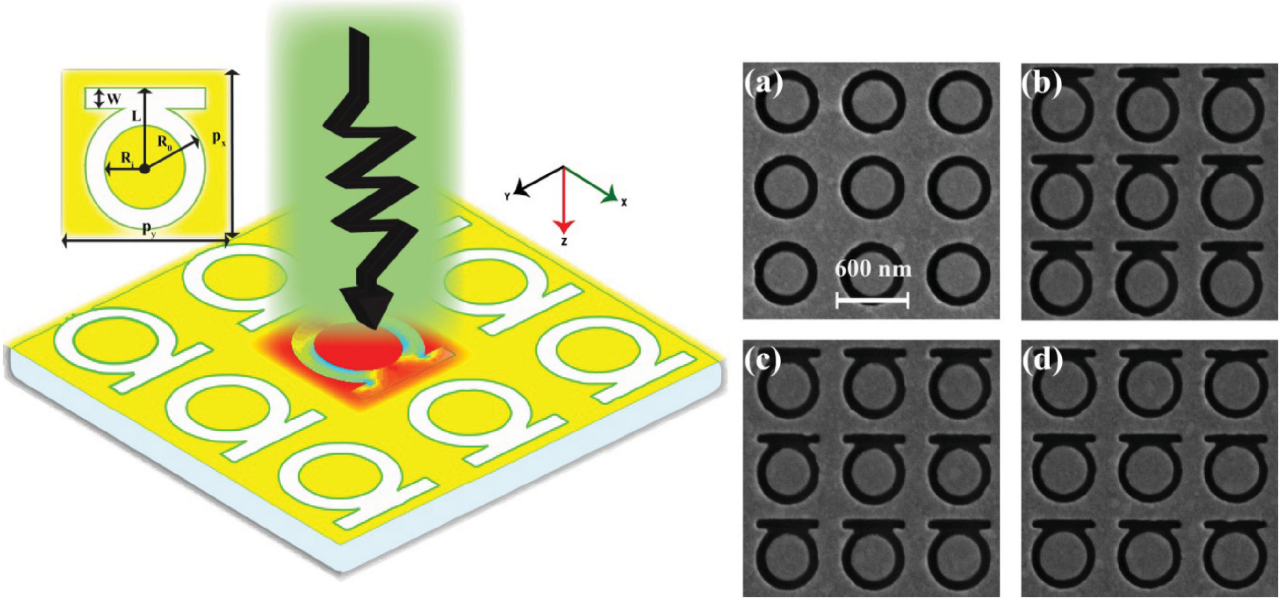

Figure 1. A schematic diagram of the overlapping annular and rectangular aperture array. The specific geometrical parameters of the unit cell are R_i = 200 nm, R_0= 300 nm, and W = 100 nm. a–d) The SEM images of the fabricated samples. The inner and outer diameter of all the samples are 400 and 600 nm, respectively, with periodicity of 800 nm in both *x* and *y* directions. Scale bar: 600 nm.

© 2016 WILEY-VCH Verlag GmbH & Co. KGaA, Weinheim

symmetric design of the annular aperture, the incident wave would couple strongly for both *x*- and *y*-polarization while the rectangular apertures array would couple efficiently for *x*-polarization and will remain dark for *y*-polarization. We found that as the annular and rectangular apertures are coupled tightly, a new sharp resonance mode with an asymmetric line shape emerges. Our experimental and simulation studies show the excitation of a strong Fano resonance line shape for *x*-polarized light due to the coupling between dipolar plasmonic mode of rectangular aperture and quadrupolar plasmonic mode of the annular aperture, and multiple Fano resonances for *y*-polarized light due to coupling of dipolar and quadrupolar plasmonic mode of rectangular aperture with the quadrupolar plasmonic mode of annular aperture. We also show that Fano resonances and their linewidth can be tuned over a wide spectral range by tailoring the coupling distance between the two resonators as the tuning parameter.

Figure 1 shows the schematic view of the proposed conductively coupled (overlapping) annular and rectangular aperture structure design. In this figure, R_i and R_0 indicate the inner and outer radius of the annular aperture, respectively, W indicates the gap width, and d represents the overlap distance between the individual annular aperture and rectangular aperture which is defined as $d = 2 * R_0 + W - L$. For our study, we fabricated arrays of connected annular and rectangular aperture structures with overlap distances d of 60, 50, and 20 nm. Focused ion beam (FIB, Helios Nanolab 600) milling has been used to fabricate the 2D arrays of nanostructures in a 50 nm thin planar gold film, deposited by thermal evaporation of gold on a quartz substrate. The size of each fabrication area has a footprint of 35 μm × 35 μm. Figure 1b–d illustrates top view of scanning electron microscopy (SEM) images of the fabricated overlapping annular and rectangular apertures, demonstrating the high quality of the well-defined patterns. The geometrical parameters of the individual annular aperture and rectangular aperture are chosen such that the dipolar mode of the individual arrays is resonant at the same frequency. For our experiment, the optimized inner and outer diameters of the fabricated annular apertures are 600 and 400 nm, respectively, and the length and width of the rectangular apertures are 600 and 100 nm. The periodicities in both directions are 800 nm.

The spectral response of the fabricated plasmonic structures at normal incidence is characterized by a Fourier transform infrared (FTIR) spectrometer coupled to an infrared confocal microscope, for both *x*- and *y*-polarization of the incident light. To probe the nature of the resonant behavior, numerical simulations using the finite-element method (COMSOL Multiphysics) are carried out to obtain the reflection spectra and the electromagnetic field distribution in the fabricated structures. In the simulated design, the permittivity of bulk gold is described by the Drude model and fused silica permittivity is 2.1. The calculated reflection spectra for the overlapping conductively coupled annular and rectangular aperture array for both polarizations show excellent agreement with the experimentally measured spectra.

3. Results

Figure 2 presents the experimental (left panel) and corresponding simulated reflection (right panel) spectra, for *x*-polarized light. Three representative annular and rectangular aperture structures with overlap distance d = 60, 50, and 20 nm, respectively are shown in Figure 1b–d, respectively. The measured reflection spectrum (purple curve) for the smallest overlap distance of 20 nm shows a broad dip at 155 THz and a characteristic asymmetric line shaped Fano resonance dip at 178 THz. In contrast to the conductively coupled structures, no pronounced Fano dip is observed for individual annular aperture array as shown in **Figure 3**. Instead, we observe a broad dip in reflection spectra at 160 THz irrespective of the incident polarization direction (magenta and blue curves of Figure 3).

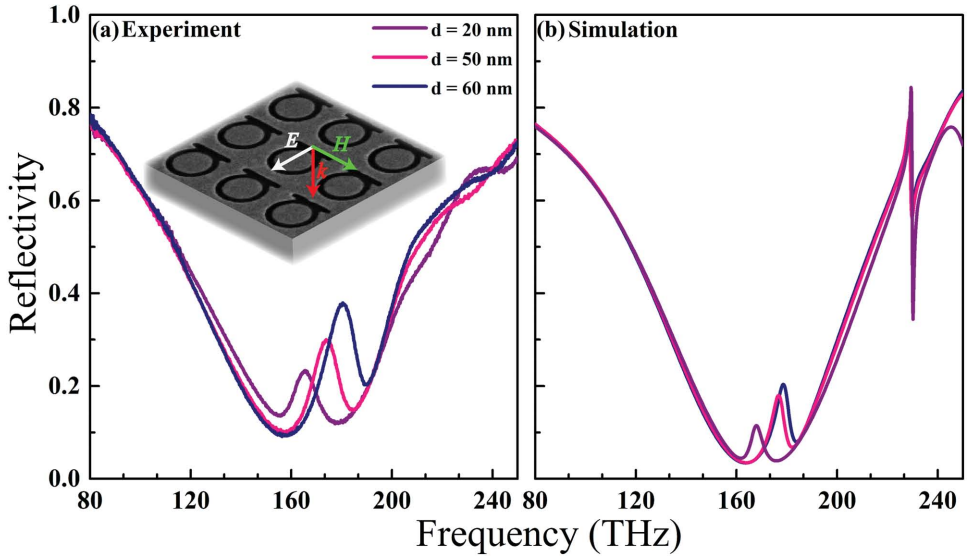

Figure 2. a) Measured and b) calculated reflection spectra for different overlapping distances between annular aperture and rectangular aperture. The polarization of the incoming light was perpendicular to the long axis of the rectangles as shown in the inset.

© 2016 WILEY-VCH Verlag GmbH & Co. KGaA, Weinheim

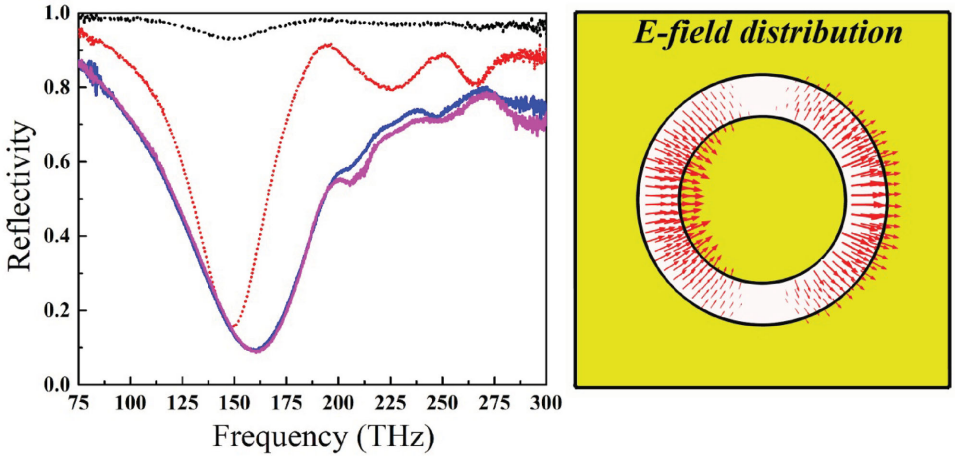

Figure 3. Left: Measured reflection spectra for individual annular aperture (solid lines) and rectangular aperture (dotted lines) array for both the polarization, perpendicular (red) and parallel (black) to the long axis of the rectangles. Right: Calculated electric field distribution in annular aperture at the resonance dip.

Similarly, for individual rectangular aperture array, we observe narrow resonance dips in the reflection spectra at 150, 225, and 265 THz. In order to gain further physical insights into the Fano resonances arising from the symmetry breaking in the hybrid annular and rectangular aperture system, we plot the simulated electric field distribution in the *x*-*y* plane of the connected annular and rectangular aperture structure at resonance frequencies of 155 and 178 THz and off resonance frequency of 200 THz. The electric field plot in **Figure 4**b illustrates the excitation of a dipolar charge distribution in the rectangular aperture and a quadrupolar charge (m = 4) distribution in the annular aperture. It can be clearly seen that the excited dipolar plasmon mode of the rectangular aperture hybridizes with the quadrupolar plasmon mode of the annular aperture, giving rise to the formation of a super-radiant mode and a sub-radiant mode with a Fano resonance at 178 THz in the reflection spectrum. It is worth noticing that in the case of only the annular aperture array, the quadrupolar mode cannot be excited under normal incidence due to the azimuthally symmetric charge distribution. However, when an asymmetry in the system is introduced through the conductively coupled rectangular aperture, a quadrupolar mode can be excited at normal incidence through the retardation effects, as indicated by the calculated charge distribution. The field distribution plot for the super-radiant mode at 155 THz shows a dipolar charge distribution in both the annular and the rectangular apertures as shown in Figure 4a. Similar well-defined azimuthally polarized modes have also been reported in coaxial groove structures by Vesseur et al.[40] Their cathodoluminescence study indicates that the circulating plasmons are plasmonic whispering gallery modes. The plasmonic whispering modes with different azimuthal mode number (m = 1, 2, ...) originate from circulating groove plasmons. For the overlap distances of 50 and 60 nm, the spectrum (pink curve and navy curve) shows approximately the same behavior as for the overlap distance of 20 nm but with a much narrower Fano dip. This tremendous sharpening effect is due to the fact that the larger overlap between annular and rectangular aperture reduces the dipole moment of the rectangular aperture considerably resulting in the lower radiative loss. Thus, the observed quality factor of the quadrupolar Fano resonance increases with enhanced coupling distance between the annular and rectangular aperture. Hence, for a given annular and rectangular aperture array, the overlap coupling distance can be tuned to accomplish the spectral tunability and lineshape narrowing of the Fano resonance dips in the reflection spectrum.

In **Figure 5**, we show the experimental and simulated reflection spectra for the incident electric field polarized along

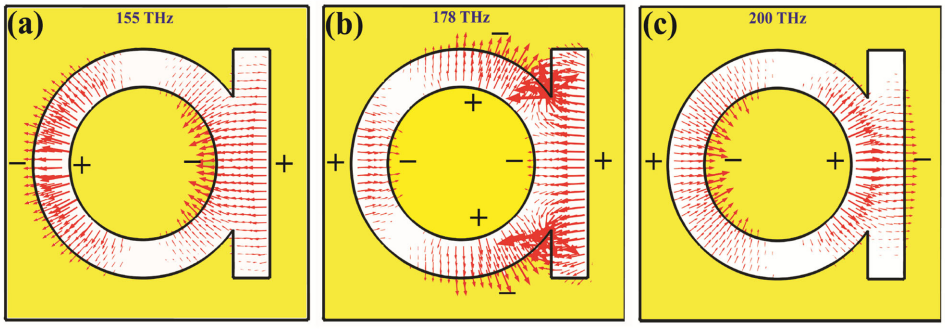

Figure 4. Simulated electric field distribution (red arrows) in the *x*-*y* plane for the overlapping annular aperture and rectangular aperture structures for *x*-polarization incidence. a,c) Dipolar mode (m = 2) and b) quadrapolar mode (m = 4) charge distributions in the annular aperture.

© 2016 WILEY-VCH Verlag GmbH & Co. KGaA, Weinheim

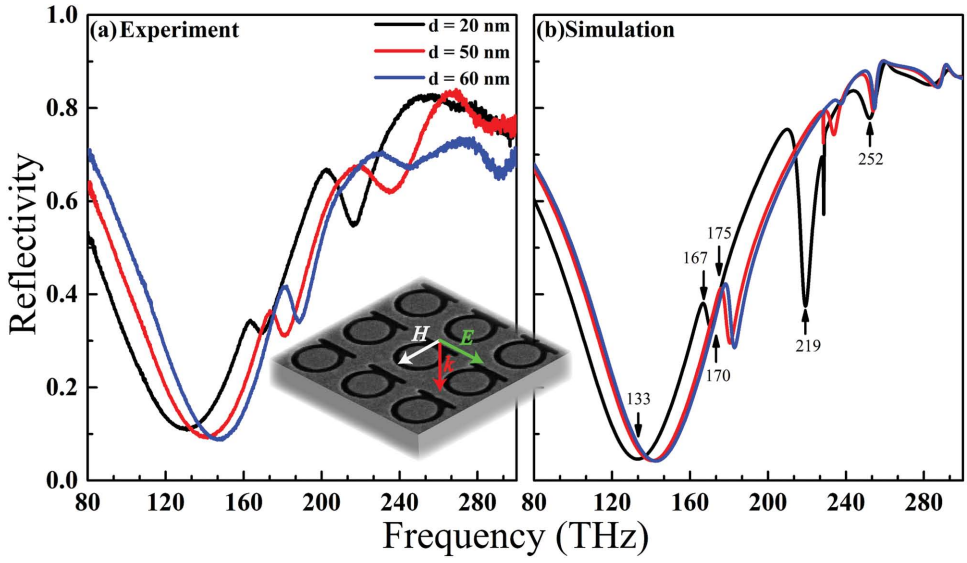

Figure 5. a) Measured and b) calculated reflection spectra for three different overlapping distances between annular aperture and rectangular aperture. The electric field of the incoming light was polarized parallel to the long axis of the rectangles as shown in the inset. The arrow marks in the simulated spectrum correspond to the frequencies of field distribution plots shown in Figure 6.

y-direction. In the case of *y*-polarized light, the measured reflection spectrum (black curve) for the overlap distance of 20 nm shows a broad dip at 133 THz and two Fano dips at 170 and 219 THz, respectively. All spectral features are reproduced in the simulation with good agreement, both in terms of the position and relative dip intensity. To clarify the appearance and properties of multiple Fano resonances, the electric field distribution at the resonance and off the resonance frequencies are plotted in **Figure 6**. As shown in the simulated electric field plot in Figure 6a, the broad reflection dip at 133 THz is caused by excitation of a dipolar charge distribution (m = 2) which is azimuthally symmetric around the annular aperture with two intense electric hot spots located in the gap of annular aperture. The electric field distribution plot for the first Fano dip, in the simulated reflection spectra, at 170 THz clearly indicate that the annular aperture has a charge distribution which results in an electric quadrupole moment (m = 4) nature with four intense electric hot spots located in the gap of annular aperture and a dipolar charge distribution in the rectangular aperture as shown in Figure 6b. The dipolar plasmon mode being excited in the rectangular aperture, which is otherwise a forbidden mode for *y*-polarization, is excited by the coherent near-field coupling that takes place between the plasmonic modes of rectangular aperture and the annular aperture. This provides a clear evidence that pronounced Fano dip is a result of the coupling between the dipole mode of rectangular aperture and the quadrupole mode of annular aperture. The additional Fano dip in the simulated reflection spectrum at 219 THz is due to the excitation of a quadrupolar charge distribution in the annular aperture structure and a quadrupolar charge distribution in the rectangular slot with two intense electric hot spots of opposite polarity, located in the rectangular slot as shown in the Figure 6c. The appearance of multiple Fano resonances are thus caused by the excitation and hybridization of dipolar and higher order modes in the rectangular aperture with higher order modes of annular aperture. A similar behavior in the reflection spectrum was observed for the structures with the overlap distances of 50 nm (red curve) and 60 nm (blue curve). We found that the dipolar mode (m = 2) and the quadrupolar mode (m = 4) resonance dips in the reflection spectrum are blue shifted to longer frequencies for the overlap distance of 50 and 60 nm.

We now dwell on the comparative study of the estimated quality factor $Q = f_0/\delta f$, where is the resonance frequency f_0 and δf is the FWHM of each dip of the Fano resonances for the case of *y*-polarized light. We compared the estimated quality factors with the *Q*-factors obtained from Fano fittings and found that the two fittings provide a consistent estimate for the *Q*-factors due to near Lorentzian nature of the resonances. The experimental quality factors of the first Fano resonance (at 170, 180, and 183THz) extracted from measured reflection dips for the overlapping distances of 60, 50, and 20 nm are 38, 33, and 31, respectively. The corresponding simulations show quality factors of 42, 36, and 31, respectively. For the second Fano resonances (at 219, 234, and 237 THz), simulated quality factors are 79, 77, and 31 for the overlapping distances of 60, 50, and 20 nm, respectively. However, in our experiment, we could only observe quality factors of 18, 13, and 16. Our simulated spectrum also show sharp resonance dips at 252 and 284 THz with quality factors of 101 and 58, respectively. From electric field distribution plot shown in Figure 6e, we notice that the quadrupolar charge distribution in the annular aperture, for the Fano resonance at 252 THz, is slightly asymmetric in comparison to the quadrupolar charge distribution at 170 THz. These features are seen in the measured spectrum but appeared to be merged in a single dip due to broadening caused by fabrication imperfections as higher order modes are extremely sensitive to the nanostructure geometry. For the case of *x*-polarized light, the experimental and numerical quality factors of Fano resonance for the overlapping distances of 60, 50, and 20 nm are 21, 18, 12 and 27, 24, 17, respectively.

In summary, we have presented an experimental and numerical study of high-*Q* Fano resonances in a novel plasmonic

© 2016 WILEY-VCH Verlag GmbH & Co. KGaA, Weinheim

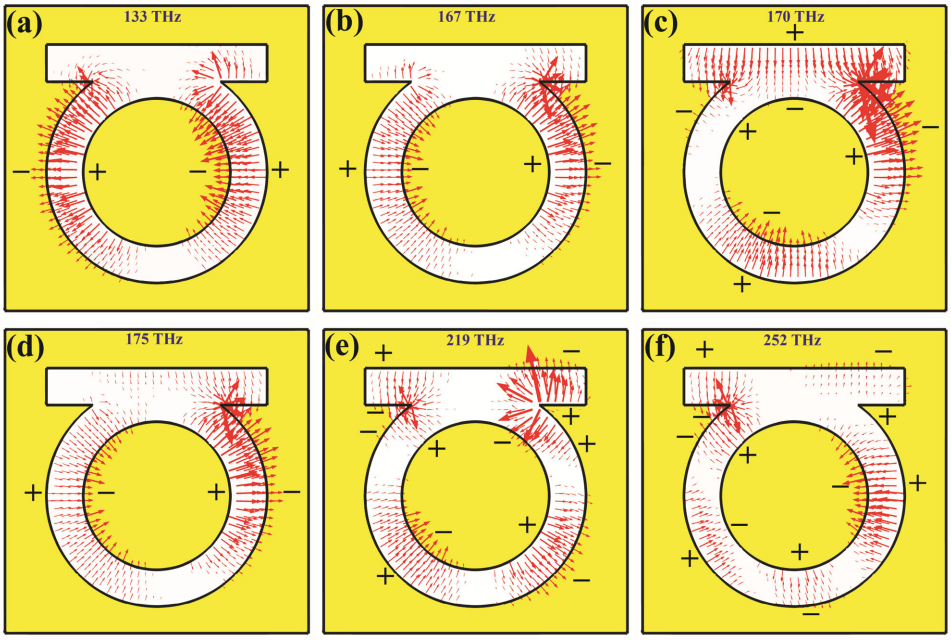

Figure 6. Simulated electric field distribution (red arrows) in the *x*-*y* plane for the overlapping annular aperture and rectangular aperture structures at respective spectral positions (as indicated by the arrows in Figure 5b) for *y*-polarization. The electric field distribution plots in (a,b,d) and (c,e,f) clearly indicate the dipolar mode ($m = 2$) and quadrupolar mode ($m = 4$) charge distributions in the annular aperture.

structure consisting of conductively coupled annular and rectangular aperture array at near infrared frequencies. Spectral tuning and narrowing of the Fano resonances were obtained by tuning the coupling distance which plays a key role in introducing the asymmetry in the system. The novelty of the present study is in the demonstration of a simple approach to tune the Fano resonances from single to multiple Fano resonances by changing the polarization of the incident radiation and making it a polarization tunable multiple Fano resonance behavior which is highly desirable for hyperspectral sensing and imaging. These high-*Q* resonances in a metallic nano structures are also desirable for efficient second harmonic generation,[41–43] biological and chemical sensing,[44–47] and slow light devices.[48]

4. Experimental Section

4.1. Fabrication

First, a 50 nm thin gold film is deposited onto a quartz substrate using thermal evaporation method (evaporation rate 0.5 Å s^{-1}). The arrays of overlapping annular and rectangular aperture are then fabricated via focused ion beam milling, carried out in a FEI Helios Nanolab 600 Dual Beam microscope system with the focused beam of gallium ions of the current of 7.7 pÅ and the energy of 30 eV. Each sample has a 35×35 μm^2 pattern area.

4.2. Simulation

The full-field electromagnetic simulations are carried out using a Finite Element Method based software package, Comsol Multiphysics. The optical properties of the metal in the simulation are characterized by a complex-frequency-dependent dielectric permittivity described by Drude free electron model $\varepsilon(\omega) = \varepsilon_\infty - \omega_p^2/(\omega^2 + i*\omega*\gamma)$ with the plasma frequency $\omega_p = 2\pi*2175$ THz and the collision frequency $\gamma = 2\pi*15$ THz. The quartz substrate is characterized by a real-frequency-independent dielectric constant n_d. In the simulation, the Floquet periodic boundary conditions are applied for the transverse boundaries of the unit cell to replicate an infinite planar array of the unit cell. Port boundary conditions are used, perpendicular to the *z*-axis, to excite a plane wave from the top of the structure with a power of 1 W. The reflection ($R(\omega)$) spectrum was calculated from S-parameters.

4.3. FTIR Measurements

The reflection spectra of the fabricated samples are recorded using a FTIR spectrometer (Bruker Vertex 80v) equipped with a confocalmicroscope (Hyperion 1000) with a liquid-nitrogen-cooled mercury cadmium telluride (MCT) detector. Reflected signals are collected with a 36× confocal objective with 0.5 NA. A ZnSe polarizer is used to polarize the incident electromagnetic field. All the spectra are recorded with a resolution of 4 cm^{-1} and 128 scans. All measurements are normalized with respect to the reflectance from a plane gold mirror.

Acknowledgements

The authors acknowledge NTU startup Grant No. M4081282, MOE Tier 1 Grant No. M4011362, and MOE Grant No. MOE2011-T3-1-005 for funding of this research.

Note: The typo in the title was corrected on August 17, 2016.

Received: May 12, 2016
Published online: June 30, 2016

[1] B. E. Sernelius, *Surface Modes in Physics*, Wiley-VCH, Berlin, Germany **2001**.
[2] S. A. Maier, *Plasmonics: Fundamentals And Applications*, Springer-Verlag, New York **2007**.

© 2016 WILEY-VCH Verlag GmbH & Co. KGaA, Weinheim

[3] S. Eustis, M. A. El-Sayed, *Chem. Soc. Rev.* **2006**, *35*, 209.
[4] K. A. Willets, R. P. Van Duyne, *Rev. Phys. Chem.* **2007**, *58*, 267.
[5] J. J. Mock, *J. Chem. Phys.* **2002**, *116*, 6755.
[6] K. Kneipp, Y. Wang, H. Kneipp, L. T. Perelman, I. Itzkan, R. Dasari, *Phys. Rev. Lett.* **1997**, *78*, 1667.
[7] P. Anger, P. Bharadwaj, L. Novotny, *Phys. Rev. Lett.* **2006**, *96*, 113002.
[8] H. Xu, E. J. Bjerneld, M. Käll, L. Börjesson, *Phys. Rev. Lett.* **1999**, *83*, 4357.
[9] H. A. Atwater, A. Polman, *Nat. Mater.* **2010**, *9*, 205.
[10] P. Andrew, W. L. Barnes, *Science* **2004**, *306*, 1002.
[11] S. Lal, S. link, N. J. Halas, *Nat. Photonics* **2007**, *1*, 641.
[12] S. Bozhevolny, *Plasmonic Nanoguides and Circuits*, Pan Stanford, Singapore **2010**.
[13] M. Aeschlimann, M. Bauer, D. Bayer, T. Brixner, F. J. Garcia de Abajo, W. Pfeiffer, M. Rohmer, C. Spindler, F. Steeb, *Nature* **2007**, *446*, 301.
[14] R. Hillenbrand, F. Keilmann, P. Hanarp, D. S. Sutherland, J. Aizpurua, *Appl. Phys. Lett.* **2003**, *83*, 368.
[15] S. Enoch, N. Bonod, *Plasmonics: From Basics to Advanced Topics*, Springer, Berlin **2012**.
[16] L. S. Slaughter, Y. P. Wu, B. Willingham, P. Nordlander, S. Link, *ACS Nano* **2010**, *4*, 4657.
[17] E. Prodan, C. Radloff, N. J. Halas, P. Nordlander, *Science* **2003**, *302*, 419.
[18] F. Neubrech, A. Pucci, T. W. Cornelius, S. Karim, A. Garcia-Etxarri, J. Aizpurua, *Phys. Rev. Lett.* **2009**, *101*, 157403.
[19] F. Le, D. W. Brandl, Y. A. Urzhumov, H. Wang, J. Kundu, N. J. Halas, J. Aizpurua, P. Nordlander, *ACS Nano* **2008**, *2*, 707.
[20] U. Fano, *Phys. Rev.* **1961**, *124*, 1866.
[21] B. Luk'yanchuk, N. I. Zheludev, S. A. Maier, N. J. Halas, P. Nordlander, H. Giessen, C. T. Chong, *Nat. Mater.* **2010**, *9*, 707.
[22] A. E. Miroshnichenko, S. Flach, Y. S. Kivshar, *Rev. Mod. Phys.* **2010**, *82*, 2257.
[23] V. A. Fedotov, M. Rose, S. L. Prosvirnin, N. Papasimakis, N. I. Zheludev, *Phys. Rev. Lett.* **2007**, *99*, 147401.
[24] F. Hao, P. Nordlander, Y. Sonnefraud, P. Van Dorpe, S. A. Maier, *ACS Nano* **2009**, *3*, 643.
[25] A. E. Cetin, H. Altug, *ACS Nano* **2012**, *6*, 9989.
[26] Y. H. Fu, J. B. Zhang, Y. F. Yu, *ACS Nano* **2012**, *6*, 5130.
[27] J. A. Fan, K. Bao, C. Wu, J. Bao, R. Bardhan, N. J. Halas, V. N. Manoharan, G. Shvets, P. Nordlander, F. Capasso, *Nano Lett.* **2010**, *10*, 4680.
[28] M. Hentschel, M. Saliba, R. Vogelgesang, H. Giessen, A. P. Alivisatos, N. Liu, *Nano Lett.* **2010**, *10*, 2721.
[29] B. Gallinet, O. J. F. Martin, *ACS Nano* **2011**, *5*, 8999.
[30] R. Singh, I. A. Al-Naib, M. Koch, W. Zhang, *Opt. Exp.* **2011**, *19*, 6312.
[31] Y. K . Srivastava, M. Manjappa, L. Cong, W. Cao, I. Al-Naib, W. Zhang, R. Singh, *Adv. Opt. Mater.* **2016**, *4*, 463.
[32] L. Cong, M. Manjappa, N. Xu, I. Al-Naib, W. Zhang, R. Singh, *Adv. Opt. Mater.* **2015**, *3*, 1543.
[33] R. Singh, I. Al-Naib, W. Cao, C. Rockstuhl, M. Koch, W. Zhang, *Terahertz Sci. Technol., IEEE Trans.* **2013**, *3*, 826.
[34] H. L. Liu, E. S. P. Leong, Z. L. Wang, G. Y. Si, L. J. Zheng, Y. J. Liu, C. Soci, *Adv. Opt. Mater.* **2013**, *1*, 978.
[35] N. Verellen, P. V. Dorpe, C. Huang, K. Lodewijks, G. A. E. Vandenbosch, L. lagae, V. V. Moschalkov, *Nano Lett.* **2011**, *11*, 391.
[36] Y. Yang, I. I. Kravchenko, D. P. Briggs, J. Valentine, *Nat. Commun.* **2014**, *5*, 5753.
[37] C. Wu, N. Arju, G. Kelp, J. A. Fan, J. Dominguez, E. Gonzales, E. Tutuc, I. Brener, G. Shvets, *Nat. Commun.* **2014**, *5*, 3892.
[38] C. Genet, T. W. Ebbesen, *Nature* **2007**, *445*, 39.
[39] W. Fan, S. Zhang, B. Minhas, K. J. Malloy, S. R. J. Brueck, *Phys. Rev. Lett.* **2005**, *94*, 033902.
[40] E. J. R. Vesseur, F. J. García de Abajo, A. Polman, *Nano Lett.* **2009**, *9*, 3147.
[41] F. Hao, Y. Sonnefraud, P. Van Dorpe, S. A. Maier, N. J. Halas, P. Nordlander, *Nano Lett.* **2008**, *8*, 3983.
[42] B. Metzger, L. Gui, J. Fuchs, D. Floess, M. Hentschel, H. Giessen, *Nano Lett.* **2015**, *15*, 3917.
[43] K. Thyagarajan, J. Butet, O. J. F. Martin, *Nano Lett.* **2013**, *13*, 1847.
[44] R. Singh, W. Cao, I. Al-Naib, L. Cong, W. Withayachumnankul, W. Zhang, *Appl. Phys. Lett.* **2014**, *105*, 171101.
[45] F. Hao, Y. Sonnefraud, P. Van Dorpe, S. A. Maier, N. J. Halas, P. Nordlander, *Nano Lett.* **2008**, *8*, 3983.
[46] T. F. Lopez, R. Paniagua Dominguez, J. A. Sanchez-Gil, *ACS Nano* **2012**, *6*, 8989.
[47] N. Verellen, Y. Sonnefraud, H. Sobhani, F. Hao, V. V. Moshchalkov, P. Van Dorpe, P. Nordlander, S. A. Maier, *Nano Lett.* **2009**, *9*,1663.
[48] C. Wu, A. B. Khanikaev, G. Shvets, *Phys. Rev. Lett.* **2011**, *106*, 107403.

© 2016 WILEY-VCH Verlag GmbH & Co. KGaA, Weinheim